Geophysical Research Letters

RESEARCH LETTER

10.1002/2015GL066675

Key Points:
- The composition of freshly deposited dust was determined on Mars
- Dust lofted on Mars today has higher S and Cl but the same S/Cl as average soil
- Air fall dust on Mars is compositionally similar across the planet

Supporting Information:
- Supporting Information S1

Correspondence to:
J. A. Berger,
jeffberger@cpsx.uwo.ca

Citation:
Berger, J. A., et al. (2016), A global Mars dust composition refined by the Alpha-Particle X-ray Spectrometer in Gale Crater, *Geophys. Res. Lett., 43*, 67–75, doi:10.1002/2015GL066675.

Received 20 OCT 2015
Accepted 11 DEC 2015
Accepted article online 22 DEC 2015
Published online 9 JAN 2016

A global Mars dust composition refined by the Alpha-Particle X-ray Spectrometer in Gale Crater

Jeff A. Berger[1], Mariek E. Schmidt[2], Ralf Gellert[3], John L. Campbell[3], Penelope L. King[3,4], Roberta L. Flemming[1], Douglas W. Ming[5], Benton C. Clark[6], Irina Pradler[3], Scott J. V. VanBommel[3], Michelle E. Minitti[7], Alberto G. Fairén[8,9], Nicholas I. Boyd[3], Lucy M. Thompson[10], Glynis M. Perrett[9], Beverley E. Elliott[10], and Elstan Desouza[3]

[1]Department of Earth Sciences, University of Western Ontario, London, Ontario, Canada, [2]Department of Earth Sciences, Brock University, St. Catharines, Ontario, Canada, [3]Guelph-Waterloo Physics Institute, University of Guelph, Guelph, Ontario, Canada, [4]Research School of Earth Sciences, Australian National University, Canberra, Australian Capital Territory, Australia, [5]Astromaterials Research and Exploration Science Directorate, NASA Johnson Space Center, Houston, Texas, USA, [6]Space Science Institute, Boulder, Colorado, USA, [7]Planetary Science Institute, Tucson, Arizona, USA, [8]Centro de Astrobiología (CSIC-INTA), Madrid, Spain, [9]Department of Astronomy, Cornell University, Ithaca, New York, USA, [10]Planetary and Space Science Centre, University of New Brunswick, Frederickton, New Brunswick, Canada

Abstract Modern Martian dust is similar in composition to the global soil unit and bulk basaltic Mars crust, but it is enriched in S and Cl. The Alpha Particle X-ray Spectrometer (APXS) on the Mars Science Laboratory *Curiosity* rover analyzed air fall dust on the science observation tray (o-tray) in Gale Crater to determine dust oxide compositions. The o-tray dust has the highest concentrations of SO_3 and Cl measured in Mars dust (SO_3 8.3%; Cl 1.1 wt %). The molar S/Cl in the dust (3.35 ± 0.34) is consistent with previous studies of Martian dust and soils (S/Cl = 3.7 ± 0.7). Fe is also elevated ~25% over average Mars soils and the bulk crust. These enrichments link air fall dust with the S-, Cl-, and Fe-rich X-ray amorphous component of Gale Crater soil. Dust and soil have the same S/Cl, constraining the surface concentrations of S and Cl on a global scale.

1. Introduction

Air fall dust is pervasive on Mars as suspended particulates in the atmosphere and as air fall deposits that coat many rock, soil, and given time, spacecraft hardware surfaces. The Martian dust cycle is closely linked to soil homogenization, with aeolian and other processes producing and mixing fine S- and Cl-rich material to form a globally homogeneous unit [*Yen et al.*, 2005, 2013]. The chemical and mineralogical makeup of the dust is therefore critically important for interpreting modern S and Cl cycles on the surface of Mars and for analyzing dusty surfaces both in situ and from orbit.

The chemical composition of Martian dust was previously estimated from Alpha-Particle X-ray Spectrometer (APXS) measurements of accumulated surface dust or air fall dust captured by rover magnets by the Pathfinder and Mars Exploration Rover (MER) missions [*Rieder et al.*, 1997; *Goetz et al.*, 2005; *Yen et al.*, 2005, 2013]. These in situ observations of Martian dust indicate a S- and Cl-rich basaltic composition with a constant molar S/Cl of 3.7 ± 0.7 (Table 1). An ambiguity in deriving dust compositions from APXS measurements of surface dust is the possible contribution from admixed aeolian fines sourced from local rocks that do not represent the air fall dust. MER magnets more likely sampled the suspended atmospheric dust and had elevated Ti, Cr, Fe, S, and Cl relative to soil; however, larger saltated grains unrepresentative of dust were observed on the magnets [*Madsen et al.*, 2003; *Bertelsen et al.*, 2004; *Goetz et al.*, 2005]. The aluminum hardware over the MER magnets prevented Al analysis as well as calculation of oxides [*Goetz et al.*, 2005].

New APXS measurements of air fall Martian dust have been possible in Gale Crater on the titanium science observation tray (o-tray), which is mounted horizontally on the front of the Mars Science Laboratory (MSL) rover, *Curiosity* (Figure S1 in the supporting information) [*Anderson et al.*, 2012]. The standard APXS calibration does not apply to the o-tray because the dust layer is thinner than the APXS sampling depth. The depth within a sample from which 90% of the X-rays are emitted (D_{90}) increases predictably with increasing atomic number (Z), ranging from ~2 μm for Na to ~90 μm for Fe in a basaltic matrix [*Rieder et al.*, 2003; *Brückner et al.*, 2008]. Air fall dust on the o-tray is uniform in thickness and composition, and thus, oxides are calculated by directly comparing the observed and modeled X-ray yields from the APXS. Here we expand on the *Curiosity*

Table 1. Elemental Compositions of In Situ Soil and O-Tray Dust in Gale Crater and Related Mars Compositions

	Gale Crater			MER		
	Soil[a]	O-tray Dust Sol 177	O-tray Dust Sol 571	Gusev Crater Dust[b]	Meridiani Planum Dust[c]	Average Martian Soil[d]
SiO_2	43.0 ± 0.5[e]	38.6 ± 4.0	39.3 ± 1.7	45.0 ± 0.5	45.0 ± 0.3	45.41
TiO_2[f]	1.10 ± 0.03	1.05 ± 0.18	1.06 ± 0.09	0.89 ± 0.08	1.01 ± 0.07	0.90
Al_2O_3	9.41 ± 0.19	9.32 ± 0.77	8.91 ± 0.39	9.56 ± 0.16	9.14 ± 0.09	9.71
FeO[g]	20.1 ± 0.3	21.6 ± 4.2	21.0 ± 2.2	16.5 ± 0.15	17.5 ± 0.04	16.73
MnO	0.42 ± 0.01	0.46 ± 0.25	0.42 ± 0.10	0.31 ± 0.02	0.34 ± 0.01	0.33
MgO	8.27 ± 0.17	8.08 ± 0.53	8.31 ± 0.38	8.25 ± 0.15	7.57 ± 0.08	8.35
CaO	7.17 ± 0.08	7.13 ± 1.23	7.04 ± 0.60	6.17 ± 0.07	6.54 ± 0.04	6.37
Na_2O	2.78 ± 0.14	2.73 ± 0.37	2.75 ± 0.22	2.9 ± 0.3	2.22 ± 0.19	2.73
K_2O	0.45 ± 0.02	0.44 ± 0.25	0.47 ± 0.09	0.49 ± 0.07	0.48 ± 0.06	0.44
P_2O_5	0.85 ± 0.05	n.d.[h]	n.d.	0.91 ± 0.09	0.93 ± 0.09	0.83
SO_3	5.12 ± 0.07	8.01 ± 0.94	8.34 ± 0.42	7.61 ± 0.13	7.28 ± 0.07	6.16
Cl	0.64 ± 0.01	1.06 ± 0.27	1.08 ± 0.12	0.88 ± 0.03	0.78 ± 0.01	0.68

[a]Disturbed soil target Sourdough Sol 673 (Figure 1).
[b]Gobi1_soil Sol 71 [*Gellert et al.*, 2006].
[c]MontBlanc_LesHauches Sol 60 [*Morris et al.*, 2006].
[d]From *Taylor and McLennan* [2010].
[e]The relative percent error shown is the larger of either the 2σ statistical fit error or the range in simulated APXS yield (Figure 2a).
[f]The Ti signal from the o-tray precludes Ti analysis; Ti in the dust is assumed to be the same as the soil (before renormalization).
[g]Total iron reported as FeO.
[h]Not detected.

dust measurements by modeling the APXS X-ray yields of a thin sample on the o-tray in order to calculate the oxide concentrations of air fall dust in Gale Crater.

2. Methods

Air fall dust on the o-tray was measured by APXS on Sols 177 and 571 (sol = 24.6 h; Figures 1 and S1). Upon landing on 6 August 2012, the MSL sky crane retrorockets lofted surface fines from a depth of several centimeters, and a thin layer settled onto the o-tray. Navigation camera (Navcam) images [*Maki et al.*, 2012] confirmed that these fines were subsequently cleaned off of the center of the o-tray by the vibration and movement of fines scooped from the Rocknest sand shadow and portioned to the o-tray for analysis (Sols 91–95) [*Berger et al.*, 2014]. The vibration and movement of fines was due to *Curiosity's* sampling subsystem vibration mechanism, which also caused the Rocknest fines to vibrate off the tray by Sol 129 [*Anderson et al.*, 2012]. On Sol 284, drill fines from a drilled mudstone target named Cumberland were portioned to the center of the tray. The drilled material had a finer grain size and was more cohesive than the scooped Rocknest fines [*Minitti et al.*, 2013], and neither wind, sampling subsystem vibrations nor rover tilt caused measureable movement of the drill fines on the o-tray. To exclude these fines from the APXS field of view (FOV) on Sol 571, the instrument was positioned ~2 cm laterally from the center of the o-tray (Figure 1b). The total dust accumulation time as of the Sol 571 measurement was between 442 and 471 sols.

Particle-induced X-ray emission (PIXE) and X-ray fluorescence (XRF) spectrometry are the basis of the APXS technique [*Gellert et al.*, 2006; *Campbell et al.*, 2012]. The MSL APXS and its related spectrum fitting code, GUAPX, are described previously [*Gellert et al.*, 2009; *Campbell et al.*, 2011a, 2011b, 2012]. Element peak areas, which are directly proportional to elemental abundances in the sample, were calculated from APXS spectra with GUAPX. Peak areas are obtained using a nonlinear least squares spectrum fitting method and are converted to element concentrations using matrix corrections, then converted to oxide concentrations whose sum is then normalized to 100 wt %. Iterations are repeated until the concentrations are consistent. Error is reported as 2σ fit error.

Because the GUAPX approach requires an infinitely thick (bulk) sample (≥1 mm), we instead derived dust oxide concentrations from the simulated X-ray yield of a thin layer of bulk soil composition on the o-tray. To do this, we used the computer code APX-Yield [*Schmidt et al.*, 2014; *Campbell et al.*, 2014; *Berger et al.*, 2014], which employs GUAPX subroutines to calculate the yield of characteristic X-rays for elements from layered samples using fundamental PIXE and XRF principles. The compositions of the thin layer and substrate

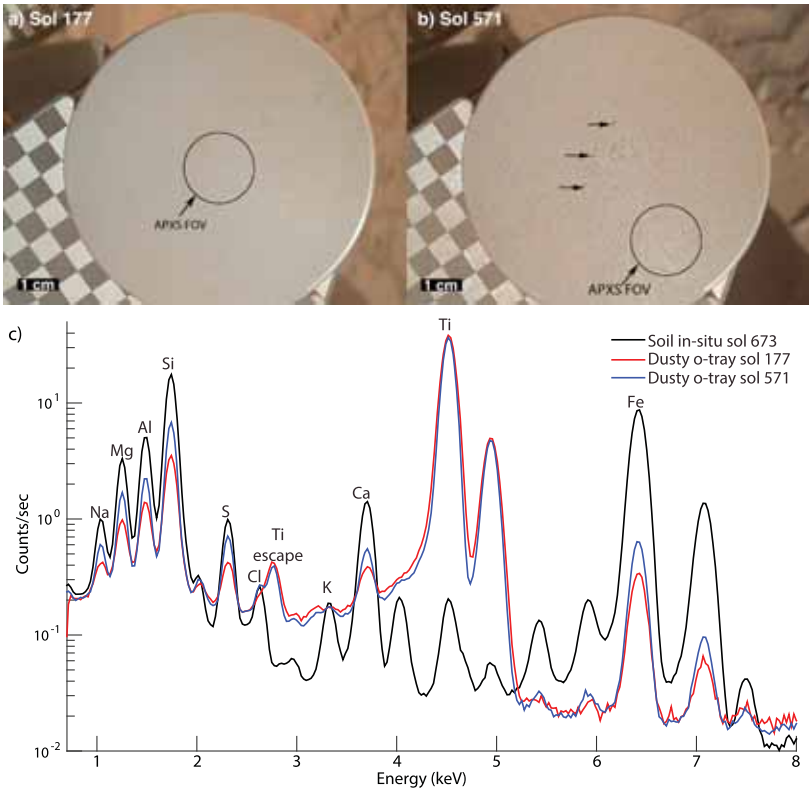

Figure 1. MAHLI images of the o-tray on Sols (a) 177 [0177MH0001320010102444E01] and (b) 571 [0571MH0003600010201899C00] and (c) APXS spectra of the dusty o-tray and in situ soil. Selected Kα and the Ti escape peaks are labeled. The ~1.7 cm diameter APXS FOV was shifted 2 cm to the right on Sol 571 to avoid the Sol 284 Cumberland drill fines in the center of the o-tray (representative drill fine aggregates indicated with smaller arrows).

are input to calculate the X-ray yield from each at a given layer thickness. Conversion of these calculated absolute X-ray yields to spectral peak areas would then require knowledge of instrumental effects such as geometric efficiency. This is not practical, and so we employ the ratios of thin samples to bulk samples, thereby removing instrumental effects. Deviations of observed thin/bulk peak area ratios from the modeled thin/bulk yield ratios are directly proportional to enrichment (or depletion) of elements in the thin sample (dust), relative to the bulk sample (soil). This is quantified by the dust correction factor DCF for each element *i*. We can thus compare elemental APXS spectral peak areas to the element APX-Yield modeled yields by the relationship

$$\mathrm{DCF}_i\left(\frac{PA_D}{PA_S}\right)_i = f_A\left(\frac{Y_D}{Y_S}\right)_i \tag{1}$$

where *PA* is the peak area, *Y* is the modeled yield, and subscripts *D* and *S* denote air fall dust and soil, respectively. The areal correction factor f_A is discussed below. This relationship allows the derivation of a dust oxide correction factor DCF

$$\mathrm{DCF}_i = f_A\left(\frac{Y_D}{Y_S}\right)_i\left(\frac{PA_S}{PA_D}\right)_i \tag{2}$$

which we used to calculate each dust oxide based on corresponding soil oxides by

$$\text{Dust oxide} = \frac{\text{Soil oxide}}{\text{DCF}} \tag{3}$$

At a given thickness, f_A is the same for all oxides. These oxide values were then renormalized to 100%. The disturbed soil target Sourdough (Sol 673; Figure S2) was used as the bulk soil because it had a

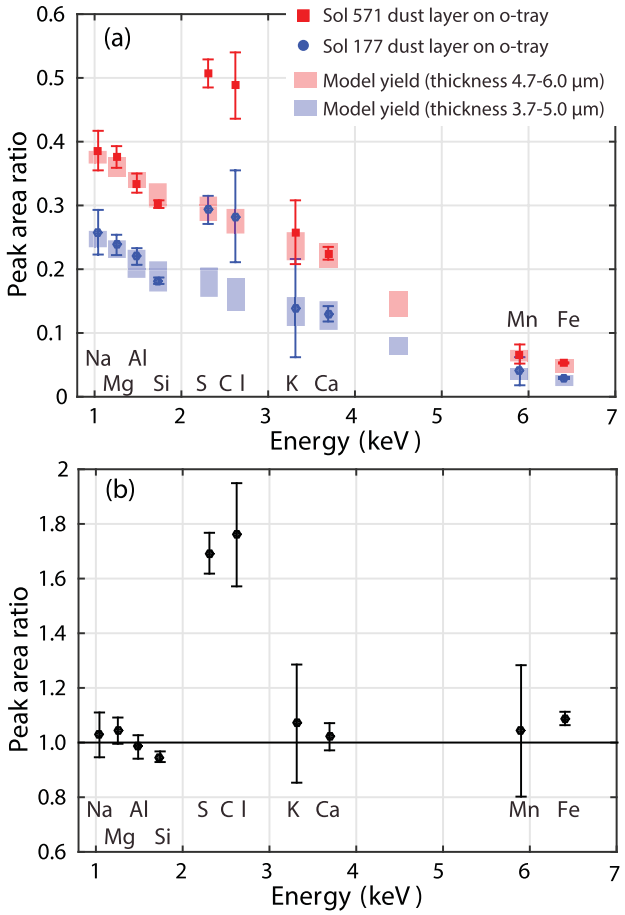

Figure 2. APXS peak areas of the dust on the o-tray, shown as ratios to (a) the peak areas of in situ, bulk soil (Sourdough; Sol 673) and (b) the modeled APXS yield of a thin layer of soil with the composition of Sourdough and a thickness of 1.1 mg/cm^2. The blue and red boxes in Figure 2a show the modeled APXS yield of a layer with soil composition. All detected elements are within the 5–10% error of the modeled yield, with the exceptions Fe, S, and Cl, which are enriched, maintaining the same S/Cl ratio as the soil.

shorter standoff distance than most other overnight soil targets and thus had better counting statistics and relatively smaller fitting error. Soil was employed as the bulk sample because it is the best first approximation of the dust composition. Any bulk sample with a similar composition would yield the same dust oxides within error; therefore, the accuracy of the technique is not sensitive to the bulk composition from which the modeled layer composition is derived.

Several assumptions were necessary to apply the APX-Yield model to measurements of dust on the o-tray. The code assumes that the layers have uniform thickness and homogeneous composition at the micrometer scale, which is reasonable for the air fall dust. Although the dust sample likely has only partial areal coverage, previous work shows that the APXS signal varies across the spectrum with changes in areal coverage and is approximately proportional to the percent areal coverage of the particulate according to the areal coverage correction factor f_A [*Berger et al.*, 2014]. We derived f_A from the Na peak area ratio (Figure 2), assuming the dust was thick with respect to the D_{90} of Na (~3 μm) [e. g., *Rieder et al.*, 2003]. The Martian dust probably formed submillimeter scale porous aggregates as it was deposited [e.g., *Johnson et al.*, 2002], which we assumed had a uniform mean thickness across the larger-scale ~1.7 cm diameter APXS FOV. The APXS signal also varies predictably with differences in instrument standoff distance, which were corrected with geometric normalization factors [*Gellert et al.*, 2006].

APXS measurements of the o-tray have additional considerations. The Ti signal from the o-tray precludes analysis of Ti in the dust, so we assumed that the TiO_2 concentrations of the dust and the soil were the same (1.1 wt %), which is consistent with apparent TiO_2 content in MER dust [*McGlynn et al.*, 2012]. Increased yields due to secondary fluorescence of Ca (6–7% increase) and K (3–4% increase) in the thin dust sample by the Ti substrate [e.g., *Berger et al.*, 2014] were modeled and corrected using APX-Yield software. Secondary fluorescence of chlorine and lighter elements due to Ti are modeled at <1% and were not corrected. APXS and laser ablation inductively coupled plasma mass spectrometry analyses of the Ti metal used for the o-tray were reported previously [*Berger et al.*, 2014]. Iron (0.24 c/s) and nickel (0.03 c/s) were the only trace elements in the Ti metal detectable by the test bed flight equivalent APXS, and these are subtracted from the dusty o-tray peak areas.

3. Results

Camera observations of the dusty o-tray on Sols 177 and 571 are consistent with a thin layer of air fall dust that increased in areal coverage, and possibly thickness, over time. Mars Hand Lens Imager (MAHLI) [*Edgett et al.*, 2012] images of the o-tray, obtained before APXS measurements during daylight hours (13:50 on Sol 177; 13:35 on Sol 571), show the dull red-brown hue of the layer of dust (Figure 1). The o-tray appears darker on Sol 571, likely due to a greater areal coverage of dust obscuring more of the light gray titanium metal. Much of the dust texture is smaller than the 60.4 μm/pixel MAHLI resolution at a 15.2 cm working distance; however, uniformly distributed rounded dust aggregates (less than ~300 μm in diameter) are apparent. At this resolution, we cannot confirm whether saltating sand particles < 200 μm were on the tray; however, modeling suggests that saltating grains ≤ 500 μm on Mars are unlikely to exceed 0.5 m in height [*Renno et al.*, 2014]. The Sol 571 o-tray image also includes linear streaks of unknown origin in the dust and indicates a change in coverage relative to Sol 177. Streaking may be evidence of aeolian pushing or rolling of dust aggregates, similar to "nick-like disturbances" observed by MER on dusty surfaces at Gusev Crater [*Sullivan et al.*, 2008]. The relative Si and Fe yields constrain the uniformity of the dust relief because they have contrasting D_{90} (~7 μm and ~90 μm, respectively). Si/Fe drops from 8.7 ± 0.3 on Sol 177 to 8.1 ± 0.2 on Sol 571, which is consistent with the modeled yield and indicates an increase in thickness with uniform coverage. Nevertheless, we increased the modeled thickness range to encompass this change in Si/Fe ratio, thus increasing the reported error to include uncertainty due to deviations in uniformity.

The APXS results indicate that the dust on the o-tray has a composition similar to that of Martian soil but with elevated FeO, SO_3, and Cl (Table 1 and Figures 1 and 2). We report Fe, S, and Cl as FeO, SO_3, and Cl, respectively, in keeping with previous literature on Martian APXS chemistry; oxidation state cannot be determined by the APXS. The APXS signal of Sol 571 dust is higher than that of Sol 177 consistent with a larger sample volume due to greater areal coverage and increased thickness. Figure 2a presents the Kα peak area ratios between the dusty o-tray and the bulk soil. For a given thickness, the progressive drop in peak area ratio with increasing Z results from the sample being thin with respect to the interrogation depth D_{90}. The Kα peak area ratios fit within the modeled yield of a layer with thicknesses 0.65–1.00 mg/cm^2 with $f_A = 0.26$ (Sol 177) and 0.95–1.20 mg/cm^2 with $f_A = 0.38$ (Sol 571) (Figure 2). Notable exceptions are S (enriched by 65–69%) and Cl (enriched by 75–76%), which have the same S/Cl value observed in the soil (Figure 2b). Trace elements (e.g., P, Ni, Zn, Br) are below detection limits owing to the small sample volume. The Sols 177 and 571 peak area ratios are within error and therefore show no significant differences between the two o-tray measurements and no evidence of contribution from the nearby Cumberland drill fines.

4. Discussion

APXS results for the dust on the o-tray in Gale Crater are congruent with the Martian dust and soil compositions observed by previous Mars rover missions [*Foley et al.*, 2003b; *Goetz et al.*, 2005; *Yen et al.*, 2005]. O-tray dust oxide values are similar to widespread, basaltic soil types examined in Gale Crater, Gusev Crater, and Meridiani Planum (e.g., Laguna Class soil) [*Ming et al.*, 2008; *Morris et al.*, 2008; *Yen et al.*, 2013], as well as by the Viking [*Clark et al.*, 1982] and Pathfinder missions [*Foley et al.*, 2003a]. Similar to six MER undisturbed soil targets at Gusev Crater and Meridiani Planum classified as "bright dust" (MER dust) [*Yen et al.*, 2005], the MSL o-tray dust also has elevated S and Cl relative to common soils and the same molar S/Cl (3.7 ± 0.7). The o-tray dust, however, has $12 \pm 3\%$ greater SO_3 and $31 \pm 11\%$ greater Cl than typical MER dust targets (Figure 3a and Table 1). Compared to MER dust and average soils, FeO is also enriched in the o-tray dust by ~25% (Figure 3b and Table 1). The Fe enrichment is smaller when compared to Gale Crater soils, which have higher FeO content (17.3–20.8 wt %) than the average value (16.7 wt %) determined from previous missions [*Taylor and McLennan*, 2010] owing to the generally higher FeO in Gale bedrock [*Schmidt et al.*, 2014]. Compositional differences between the o-tray dust and MER dust likely result from the different sampling and measurement conditions. The MER dust was measured on undisturbed ground surfaces that had accumulated dust over an unknown amount of time; it is uncertain how accurately the surface dust represents atmospheric dust because saltating and creeping fines may have mixed with the surface dust [e.g., *McGlynn et al.*, 2011]. The influence of local materials is also evident in the skew of the MER dust oxide values toward the local soils (Figure 3). Nonetheless, the compositional similarities of the o-tray air fall dust, surface dust, and typical Martian soils link the materials on a global scale.

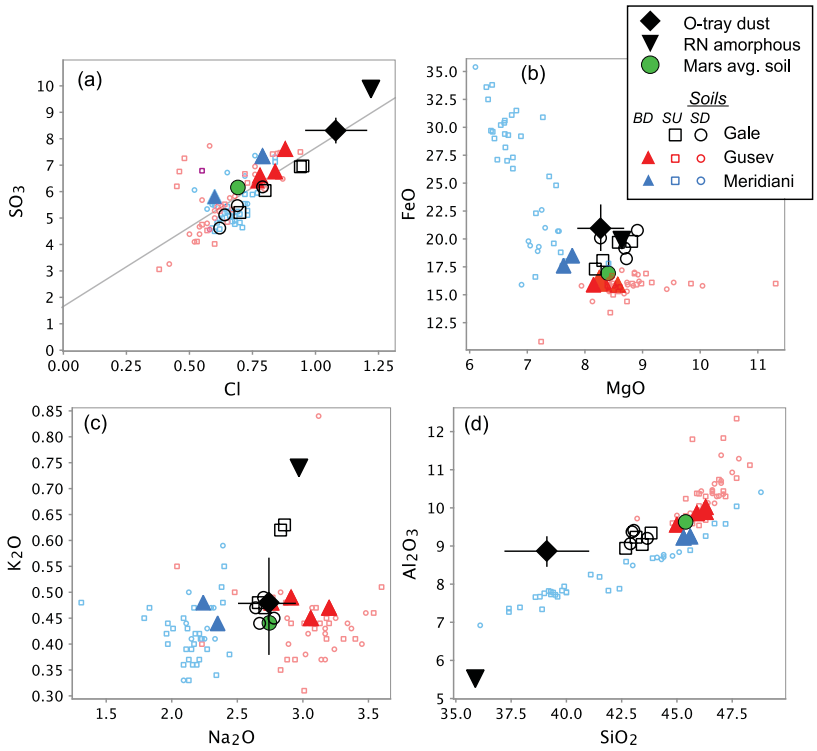

Figure 3. Martian dust composition relative to soils in Gale Crater, Gusev Crater, and Meridiani Planum (wt %). The estimated XRD amorphous component of Rocknest aeolian fines (RN amorphous) is plotted [*Morris et al.*, 2015]. Bright dust (BD), undisturbed soil (SU), and disturbed soil (SD) are indicated. The estimated average Mars soil composition is shown (green circle) [*Taylor and McLennan*, 2010]. Silica- and sulfate-rich MER soils are omitted. Error is shown for the o-tray dust and is contained within the symbols for Gale soils and MER bright dust. Error is not shown for MER soils but is similar to Gale soils.

Curiosity's investigation of the aeolian sand shadow named Rocknest (Sols 57–100) constrains the dust chemistry and mineralogy because the scooped and sieved material (<150 μm) delivered to onboard instruments likely contained a fraction of dust. Such accumulations of aeolian sediment are commonly a mixture of sand and dust that retain the compositional characteristics of local and regional rocks as well as atmospheric dust [e.g., *Bagnold*, 1941; *Bishop et al.*, 2002; *Bridges and Muhs*, 2012]. In the o-tray dust, no elements quantified by APXS ($Z \geq 11$) exhibit the same magnitude of enrichment as S and Cl (Figure 2b), indicating that the two are not each bonded with a single cation (Na^+, K^+, Mg^{2+}, Ca^{2+}, Fe^{2+}, and Fe^{3+}) in one salt phase. S and Cl may instead be adsorbed ions, coordinated with lighter elements (e.g., perchlorate), and/or distributed in a mixture of multiple salt phases (e.g., Mg-, Ca-sulfates, and halite). One S-bearing crystalline phase, anhydrite (1.5 ± 0.7 wt %), was detected in the Rocknest deposit by the Chemistry and Mineralogy (CheMin) X-ray diffraction (XRD) instrument, but it does not account for all of the SO_3 measured by APXS (5.5 ± 0.1 wt %) [*Bish et al.*, 2013]. Similarly, evolved gas analysis (EGA) by the Sample Analysis at Mars instrument (SAM) yielded the equivalent of 0.5–3.5 wt % SO_3 in both oxidized and reduced sulfur compounds consistent with minor amounts of sulfides and sulfates/sulfites [*McAdam et al.*, 2014]. The remaining ~3 wt % SO_3 could be associated with an X-ray amorphous phase (see below) [*McAdam et al.*, 2014]. Oxychlorine compounds (e.g., perchlorates and chlorates) detected by SAM in the Rocknest deposit at 0.3–0.5 wt % ClO_4^- account for much but not all of the Cl detected by APXS (0.69 ± 0.03 wt %) [*Glavin et al.*, 2013; *Leshin et al.*, 2013]. Neither halides nor Ca- or Mg-perchlorates were present above the CheMin detection limit (1–2 wt %) [*Bish et al.*, 2013]. Chlorine in APXS analyses of Gale Crater rocks is also correlated with oxychlorine compounds inferred from SAM measurements [*Archer et al.*, 2015], confirming they are stable at the Martian surface in modern aeolian deposits as well as in mudstones deposited before 1.6 Ga [*Farley et al.*, 2014]. Oxychlorine compounds can be formed via multiple pathways, including oxidation reactions in the atmosphere involving aerosols [*Catling et al.*, 2010]; therefore, they are likely a Cl-bearing phase in the dust.

A substantial fraction of the Rocknest sample (~45–50 wt %) was amorphous (i.e., without coherent X-ray diffraction), as determined by CheMin [*Blake et al.*, 2013; *Morris et al.*, 2015]. The relative proportions of crystalline phases, along with the bulk chemistry of Rocknest (represented by the APXS target Portage; Sol 89 [*Gellert et al.*, 2013]), enable mass balance calculations which indicate that most of the S and Cl, and much of the Fe, are contained in the amorphous fraction (Figure 3) [*Blake et al.*, 2013; *Dehouck et al.*, 2014; *Morris et al.*, 2015]. The crystalline component of Rocknest accounts for ~50 wt % of the Fe_{Total} ($Fe + FeO + Fe_2O_3$), primarily as FeO in basaltic minerals, and the remainder is associated with the amorphous fraction [*Bish et al.*, 2013]. Because the amorphous component of Rocknest contains most of the S and Cl in the aeolian deposit, and a significant fraction of the Fe, it is likely closely related to the air fall dust, which is also elevated in these three elements relative to typical Martian soils.

Approximately 20 wt % of the amorphous component of Rocknest is Fe_{Total}, indicating the presence of an X-ray amorphous ferric nanophase oxide (npOx) [*Blake et al.*, 2013; *Morris et al.*, 2015]. This is consistent with the presence of npOx in soils at Gusev Crater and Meridiani Planum, where npOx in the dust is yet higher [*Morris et al.*, 2006, 2008, 2013]. Mössbauer mineralogy of MER soils shows a positive correlation of Fe^{3+}/Fe_{Total} with SO_3 in the basaltic Laguna Class soils at a ratio of 0.051 ± 0.009 ($R^2 = 0.52$) [*Morris et al.*, 2008]. *Curiosity* does not have a Mössbauer instrument, and the APXS cannot measure Fe oxidation state; however, assuming this relationship extends to Gale Crater soils and dust [e.g., *Morris et al.*, 2013], we extrapolated possible Fe^{3+}/Fe_{Total} values based on SO_3 content to calculate Fe_2O_3 for Gale Crater soils and the o-tray dust (Figure S3). The estimated Fe_2O_3 values for Gale Crater indicate a positive correlation between ferric Fe and both SO_3 and Cl ($R^2 = 0.90$ and 0.82, respectively). This suggests that the three elements are associated, maintaining consistent S/Fe^{3+} and Cl/Fe^{3+} ratios in the soil, dust, and amorphous fraction. The Fe, S, and Cl are most enriched in the amorphous material, with dust intermediate between that and soils. We emphasize that this conclusion is based on an assumption about oxidation state that cannot be verified with the APXS, and we do not infer that the dust and the amorphous material are necessarily the same. Nevertheless, the similarity of S/Cl at the three distant Mars rover sites couples the Fe, S, and Cl enrichments in the o-tray dust to the gradational positive correlations between S, Cl, and Fe^{3+}/Fe_{Total} in MER soils and dust. This is evidence that the global dust is enriched in npOx associated with S and Cl, which is mixed into the soils, and, therefore, dust is a key part of soil-forming processes and the distribution of Fe, S, and Cl on the Martian surface.

The global compositional similarities of soil and dust support models of the dust cycle and soil formation that include the global circulation of dust [*McSween and Keil*, 2000; *Bishop et al.*, 2002; *McGlynn et al.*, 2011]. Aeolian processes suspend the finest fraction of surface fines (1.4–2.5 μm) [*Clancy et al.*, 2003], which is mixed in the atmosphere by local dust devils and seasonal, regional dust storms. Global dust storms are less well understood but occur approximately every 1–3 Mars years [*Liu et al.*, 2003] (1 Mars year = 687 days). The dust is redeposited to the surface by settling where it can be remixed into the soil by aeolian processes [e.g., *McGlynn et al.*, 2011]. The arid Martian climate enhances dust availability, in contrast to Earth where it is restricted by widespread liquid water, preventing global dust storms [*Rafkin et al.*, 2013]. On Mars, the dust distributes the S- and Cl-bearing fines globally and thus is an active S and Cl cycling process at the surface.

5. Conclusion

APXS results for the dust on the *Curiosity* rover o-tray in Gale Crater represent a refinement of the Martian global dust compositions observed by previous Mars missions. As observed around the planet, Martian dust has a globally uniform composition related to soils. The dust is enriched in S, Cl, and Fe relative to typical soils but with the same S/Cl ratio (~3.7). These observations support models that link the global dust cycle and soil formation, where the fine dust is globally distributed by aeolian processes and is input to the surface where it becomes a component of the soil. The dust is thus an important agent for distributing S and Cl globally to the surface of modern Mars.

Acknowledgments

APXS data are available at the planetary data system: http://pds-geosciences.wustl.edu/missions/msl/apxs.htm. The MSL APXS is managed and financed by the Canadian Space Agency (CSA), with MDA as prime contractor. Science team funding is provided by CSA and NASA/JPL-Caltech. A CSA MSL Participating Scientist Grant awarded to Schmidt supported Berger. Berger was also supported by an NSERC CREATE fellowship and two contracts from NASA/JPL-Caltech to King. King was supported by a CSA grant 9F052-10-0802 and an Australian Research Council grant FT130101524. Development by Campbell of the APX-Yield software was supported by CSA grant 09-SCIGRA-37.

References

Anderson, R. C., et al. (2012), Collecting samples in Gale Crater, Mars; An overview of the Mars Science Laboratory sample acquisition, sample processing and handling system, *Space Sci. Rev.*, *170*(1–4), 57–75, doi:10.1007/s11214-012-9898-9.

Archer, P. D., et al. (2015), Oxychlorine species on Mars: The Gale Crater story, vol. 46, p. 2971.

Bagnold, R. A. (1941), *The Physics of Blown Sand and Desert Dunes*, William Morrow, London, Reprinted (1960), Methuen and Co. Ltd., London.

Berger, J. A., et al. (2014), MSL-APXS titanium observation tray measurements: Laboratory experiments and results for the Rocknest fines at the Curiosity field site in Gale Crater, Mars, *J. Geophys. Res. Planets*, *119*, 1046–1060, doi:10.1002/2013JE004519.
Bertelsen, P., et al. (2004), Magnetic properties experiments on the Mars Exploration Rover Spirit at Gusev Crater, *Science*, *305*(5685), 827–829, doi:10.1126/science.1100112.
Bish, D. L., et al. (2013), X-ray diffraction results from Mars Science Laboratory: Mineralogy of Rocknest at Gale Crater, *Science*, *341*(6153), 1238932, doi:10.1126/science.1238932.
Bishop, J. L., S. L. Murchie, C. M. Pieters, and A. P. Zent (2002), A model for formation of dust, soil, and rock coatings on Mars: Physical and chemical processes on the Martian surface, *J. Geophys. Res.*, *107*(E11), 5097, doi:10.1029/2001JE001581.
Blake, D. F., et al. (2013), Curiosity at Gale Crater, Mars: Characterization and analysis of the Rocknest sand shadow, *Science*, *341*(6153), 1239505, doi:10.1126/science.1239505.
Bridges, N. T., and D. R. Muhs (2012), Duststones on Mars: Source, transport, deposition, and erosion, *Sediment. Geol. Mars*, *102*, 169–182.
Brückner, J., G. Dreibus, R. Gellert, S. W. Squyres, H. Wänke, A. Yen, and J. Zipfel (2008), Mars Exploration Rovers: Chemical composition by the APXS, in *The Martian Surface*, vol. 1, edited by J. F. Bell III, pp. 58–101, Cambridge Univ. Press, New York.
Campbell, J. L., J. A. Maxwell, S. M. Andrushenko, S. M. Taylor, B. N. Jones, and W. Brown-Bury (2011a), A GUPIX-based approach to interpreting the PIXE-plus-XRF spectra from the Mars Exploration Rovers: I. Homogeneous standards, *Nucl. Instrum. Methods Phys. Res., Sect. B*, *269*(1), 57–68, doi:10.1016/j.nimb.2010.10.004.
Campbell, J. L., A. M. McDonald, G. M. Perrett, and S. M. Taylor (2011b), A GUPIX-based approach to interpreting the PIXE-plus-XRF spectra from the Mars Exploration Rovers: II geochemical reference materials, *Nucl. Instrum. Methods Phys. Res., Sect. B*, *269*(1), 69–81, doi:10.1016/j.nimb.2010.09.014.
Campbell, J. L., G. M. Perrett, R. Gellert, S. M. Andrushenko, N. I. Boyd, J. A. Maxwell, P. L. King, and C. D. M. Schofield (2012), Calibration of the Mars Science Laboratory Alpha Particle X-ray Spectrometer, *Space Sci. Rev.*, *170*(1–4), 319–340, doi:10.1007/s11214-012-9873-5.
Campbell, J. L., et al. (2014), The Mars Science Laboratory APXS calibration target: Comparison of Martian measurements with the terrestrial calibration, *Nucl. Instrum. Methods Phys. Res., Sect. B*, *323*, 49–58, doi:10.1016/j.nimb.2014.01.011.
Catling, D. C., M. W. Claire, K. J. Zahnle, R. C. Quinn, B. C. Clark, M. H. Hecht, and S. Kounaves (2010), Atmospheric origins of perchlorate on Mars and in the Atacama, *J. Geophys. Res.*, *115*, E00E11, doi:10.1029/2009JE003425.
Clancy, R. T., M. J. Wolff, and P. R. Christensen (2003), Mars aerosol studies with the MGS TES emission phase function observations: Optical depths, particle sizes, and ice cloud types versus latitude and solar longitude, *J. Geophys. Res.*, *108*(E9), 5098, doi:10.1029/2003JE002058.
Clark, B. C., A. K. Baird, R. J. Weldon, D. M. Tsusaki, L. Schnabel, and M. P. Candelaria (1982), Chemical composition of Martian fines, *J. Geophys. Res.*, *87*(B12), 10,059–10,067, doi:10.1029/JB087iB12p10059.
Dehouck, E., S. M. McLennan, P.-Y. Meslin, and A. Cousin (2014), Constraints on abundance, composition, and nature of X-ray amorphous components of soils and rocks at Gale Crater, Mars, *J. Geophys. Res. Planets*, *119*, 2640–2657, doi:10.1002/2014JE004716.
Edgett, K. S., et al. (2012), Curiosity's Mars Hand Lens Imager (MAHLI) investigation, *Space Sci. Rev.*, *170*(1–4), 259–317, doi:10.1007/s11214-012-9910-4.
Farley, K. A., et al. (2014), In situ radiometric and exposure age dating of the Martian surface, *Science*, *343*(6169), 1247166, doi:10.1126/science.1247166.
Foley, C. N., T. E. Economou, R. N. Clayton, and W. Dietrich (2003a), Calibration of the Mars Pathfinder alpha proton X-ray spectrometer, *J. Geophys. Res.*, *108*(E12), 8095, doi:10.1029/2002JE002018.
Foley, C. N., T. Economou, and R. N. Clayton (2003b), Final chemical results from the Mars Pathfinder alpha proton X-ray spectrometer, *J. Geophys. Res.*, *108*(E12), 8096, doi:10.1029/2002JE002019.
Gellert, R., et al. (2006), Alpha Particle X-Ray Spectrometer (APXS): Results from Gusev Crater and calibration report, *J. Geophys. Res.*, *111*, E02S05, doi:10.1029/2005JE002555.
Gellert, R., J. L. Campbell, P. L. King, L. A. Leshin, G. W. Lugmair, J. G. Spray, S. W. Squyres, and A. S. Yen (2009), The Alpha-Particle-X-Ray-Spectrometer (APXS) for the Mars Science Laboratory (MSL) rover mission, in *Lunar Planet. Sci., XL*, Abstract 2364.
Gellert, R., et al. (2013), Initial MSL APXS activities and observations at Gale Crater, Mars, in *Lunar Planet. Sci., XLIV*, Abstract 1432.
Glavin, D. P., et al. (2013), Evidence for perchlorates and the origin of chlorinated hydrocarbons detected by SAM at the Rocknest aeolian deposit in Gale Crater, *J. Geophys. Res. Planets*, *118*, 1955–1973, doi:10.1002/jgre.20144.
Goetz, W., et al. (2005), Indication of drier periods on Mars from the chemistry and mineralogy of atmospheric dust, *Nature*, *436*(7047), 62–65, doi:10.1038/nature03807.
Johnson, J. R., P. R. Christensen, and P. G. Lucey (2002), Dust coatings on basaltic rocks and implications for thermal infrared spectroscopy of Mars, *J. Geophys. Res.*, *107*(E6), 5035, doi:10.1029/2000JE001405.
Leshin, L. A., et al. (2013), Volatile, isotope, and organic analysis of Martian fines with the Mars Curiosity Rover, *Science*, *341*(6153), 1238937, doi:10.1126/science.1238937.
Liu, J., M. I. Richardson, and R. J. Wilson (2003), An assessment of the global, seasonal, and interannual spacecraft record of Martian climate in the thermal infrared, *J. Geophys. Res.*, *108*(E8), 5089, doi:10.1029/2002JE001921.
Madsen, M. B., et al. (2003), Magnetic properties experiments on the Mars Exploration Rover mission, *J. Geophys. Res.*, *108*(E12), 8069, doi:10.1029/2002JE002029.
Maki, J., D. Thiessen, A. Pourangi, P. Kobzeff, T. Litwin, L. Scherr, S. Elliott, A. Dingizian, and M. Maimone (2012), The Mars Science Laboratory engineering cameras, *Space Sci. Rev.*, *170*(1–4), 77–93, doi:10.1007/s11214-012-9882-4.
McAdam, A. C., et al. (2014), Sulfur-bearing phases detected by evolved gas analysis of the Rocknest aeolian deposit, Gale Crater, Mars, *J. Geophys. Res. Planets*, *119*, 373–393, doi:10.1002/2013JE004518.
McGlynn, I. O., C. M. Fedo, and H. Y. McSween (2011), Origin of basaltic soils at Gusev Crater, Mars, by aeolian modification of impact-generated sediment, *J. Geophys. Res.*, *116*, E00F22, doi:10.1029/2010JE003712.
McGlynn, I. O., C. M. Fedo, and H. Y. McSween (2012), Soil mineralogy at the Mars Exploration Rover landing sites: An assessment of the competing roles of physical sorting and chemical weathering, *J. Geophys. Res.*, *117*, E01006, doi:10.1029/2011JE003861.
McSween, H. Y., Jr., and K. Keil (2000), Mixing relationships in the Martian regolith and the composition of globally homogeneous dust, *Geochim. Cosmochim. Acta*, *64*(12), 2155–2166, doi:10.1016/S0016-7037(99)00401-9.
Ming, D. W., et al. (2008), Geochemical properties of rocks and soils in Gusev Crater, Mars: Results of the Alpha Particle X-Ray Spectrometer from Cumberland Ridge to Home Plate, *J. Geophys. Res.*, *113*, E12S39, doi:10.1029/2008JE003195.
Minitti, M. E., et al. (2013), MAHLI at the Rocknest sand shadow: Science and science-enabling activities, *J. Geophys. Res. Planets*, *118*, 2338–2360, doi:10.1002/2013JE004426.
Morris, R. V., et al. (2006), Mössbauer mineralogy of rock, soil, and dust at Meridiani Planum, Mars: Opportunity's journey across sulfate-rich outcrop, basaltic sand and dust, and hematite lag deposits, *J. Geophys. Res.*, *111*, E12S15, doi:10.1029/2006JE002791.

Morris, R. V., et al. (2008), Iron mineralogy and aqueous alteration from Husband Hill through Home Plate at Gusev Crater, Mars: Results from the Mössbauer instrument on the Spirit Mars Exploration Rover, *J. Geophys. Res.*, *113*, E12S42, doi:10.1029/2008JE003201.
Morris, R. V. et al. (2013), The amorphous component in Martian basaltic soil in global perspective from MSL and MER missions, in *Lunar Planet. Sci., XLIV*, Abstract 1653.
Morris, R. V., et al. (2015), Update on the chemical composition of crystalline, smectite, and amorphous components for Rocknest soil and John Klein and Cumberland mudstone drill fines at Gale Crater, Mars, in *Lunar Planet. Sci., XLVI*, 16–20 Mar. 2015, United States.
Rafkin, S. C. R., J. L. Hollingsworth, M. A. Mischna, C. E. Newman, and M. I. Richardson (2013), Mars: Atmosphere and climate overview, *Comp. Climatol. Terr. Planets*, *1*, 55–89.
Renno, N. O., D. Halleaux, H. Elliott, and J. F. Kok (2014), The lifting of aerosols and their effects on atmospheric dynamics, *Comp. Climatol. Terr. Planets*, *355*.
Rieder, R., T. Economou, H. Wänke, A. Turkevich, J. Crisp, J. Brückner, G. Dreibus, and H. Y. McSween (1997), The chemical composition of Martian soil and rocks returned by the mobile Alpha Proton X-ray Spectrometer: Preliminary results from the X-ray mode, *Science*, *278*(5344), 1771–1774, doi:10.1126/science.278.5344.1771.
Rieder, R., R. Gellert, J. Brückner, G. Klingelhöfer, G. Dreibus, A. Yen, and S. W. Squyres (2003), The new Athena Alpha Particle X-ray Spectrometer for the Mars Exploration Rovers, *J. Geophys. Res.*, *108*(E12), 8066, doi:10.1029/2003JE002150.
Schmidt, M. E., et al. (2014), Geochemical diversity in first rocks examined by the Curiosity Rover in Gale Crater: Evidence for and significance of an alkali and volatile-rich igneous source, *J. Geophys. Res. Planets*, *119*, 64–81, doi:10.1002/2013JE004481.
Sullivan, R., R. Arvidson, J. F. Bell, R. Gellert, M. Golombek, R. Greeley, K. Herkenhoff, J. Johnson, S. Thompson, and P. Whelley (2008), Wind-driven particle mobility on Mars: Insights from Mars Exploration Rover observations at "El Dorado" and surroundings at Gusev Crater, *J. Geophys. Res.*, *113*, E06S07, doi:10.1029/2008JE003101.
Taylor, S. R., and S. McLennan (2010), *Planetary Crusts: Their Composition, Origin and Evolution*, 1st ed., Cambridge Univ. Press, Cambridge.
Yen, A. S., et al. (2005), An integrated view of the chemistry and mineralogy of Martian soils, *Nature*, *436*(7047), 49–54, doi:10.1038/nature03637.
Yen, A. S., et al. (2013), Evidence for a global Martian soil composition extends to Gale Crater, in *Lunar Planet. Sci., XLIV*, Abstract 2495.